Geomechanics and Engineering, *Vol. 34, No. 3 (2023) 251-265*
https://doi.org/10.12989/gae.2023.34.3.251

Investigation of crack growth in a brick masonry wall due to twin perpendicular excavations

Mukhtiar Ali Soomro*[1], Dildar Ali Mangnejo[2] and Naeem Mangi[3]

[1]*School of Mechanics and Civil Engineering, China University of Mining and Technology, Xuzhou, Jiangsu, P. R. China*
[2]*Department of Civil Engineering, Mehran University of Engineering and Technology, Shaheed Zulfiqar Ali Bhutto Campus, Khairpur Mir's, Sindh, Pakistan*
[3]*Department of Civil Engineering, Quaid-e-Awam University of Engineering, Science & Technology, Sindh, Pakistan*

(*Received February 11, 2023, Revised June 17, 2023, Accepted June 23, 2023*)

Abstract. In urban construction projects, it is crucial to evaluate the impacts of excavation-induced ground movements in order to protect surrounding structures. These ground movements resulting in damages to the neighboring structures and facilities (i.e., parking basement) are of main concern for the geotechnical engineers. Even more, the danger exists if the nearby structure is an ancient or masonry brick building. The formations of cracks are indicators of structural damage caused by excavation-induced ground disturbances, which pose issues for excavation-related projects. Although the effects of deep excavations on existing brick masonry walls have been thoroughly researched, the impact of twin excavations on a brick masonry wall is rarely described in the literature. This work presents a 3D parametric analysis using an advanced hypoplastic model to investigate the responses of an existing isolated brick masonry wall to twin perpendicular excavations in dry sand. One after the other, twin perpendicular excavations are simulated. This article also looks at how varying sand relative densities (D_r = 30%, 50%, 70%, and 90%) affect the masonry wall. The cracks at the top of the wall were caused by the hogging deformation profile caused by the twin excavations. By raising the relative density from 30% to 90%, excavation-induced footing settlement is greatly minimized. The crack width at the top of the wall reduces as a result of the second excavation in very loose to loose sand (D_r = 30% and 50%). While the crack width on the top of the wall increases owing to the second excavation in medium to very dense sand (D_r = 70% and 90%).

Keywords: damage; masonry wall; parametric study; twin excavations

1. Introduction

Deep excavations are often used in urban areas, such as underground transport systems and basements for car parking (Lee 2019, Shi *et al.* 2019, Ding *et al.* 2017). Since the deep excavation inevitably induces unfavorable movement and stress changes in the ground, it can cause additional settlement and cracks to nearby existing structures, especially in masonry buildings. Hence, excavation remains a big challenge for geotechnical engineers, particularly when an excavation is to be carried out adjacent to the load-bearing structure. Therefore, it is vital to predict the damages in masonry wall due to an adjacent excavation so as measures can be taken to minimize the impact of the ground deformation. Damage levels have been investigated and developed for buildings adjacent to excavation-induced stress release by performing physical scaled model tests (Ou *et al.* 2000, Giardina *et al.* 2012), analytical approaches (Halim and Wong 2012, Basmaji *et al.* 2019), field observations, case studies (Son and Cording 2005), 2D numerical analyses (Son and Cording 2008, 2011, Hashemi *et al.* 2015, Karira *et al.* 2022), and also 3D numerical simulations (Minh 2013, Giardina *et al.* 2010, 2013, 2015, Lin *et al.* 2014, Orazalin *et al.* 2015, Zhang *et al.* 2016, Dong *et al.*2017, Bejarano-Urrego *et al.* 2018, Lasciarrea *et al.* 2019). The different methods are also addressed in the literature by focusing on the ground surface settlement and horizontal strain of building frames (Ghahreman 2004, Naeimifar *et al.* 2021), differential settlement of building frames (Halim and Wong 2012), and lateral strain and angular distortion of building walls (Schuster *et al.* 2009) to classify damage levels in buildings. The underground transportation systems and basements for parking provided in the buildings have become common; it is sometimes unavoidable to encounter double neighbouring excavations adjacent to the buildings (Shi *et al.* 2020, Ruan *et al.* 2010, Wu 2012, Shen 2012, Mu *et al.* 2021, Jamil and Ahmad 2019). Chen *et al.* (2013) described a case history of two excavations at the same time in Shanghai soft clay. It was found that the displacements of the wall between the two excavations were larger than those of other sides, which might be due to the surcharge. The maximum settlement was about 0.18% of the excavation depth. Numerical analyses have been conducted to investigate the soil and wall deformation during several excavations by some researchers (Ruan *et al.* 2010, Wu 2012, Shen 2012, Qian *et al.* 2020, Soomro *et al.* 2022c).

They found that the soil settlements during several excavations were larger than the superimposed settlements in each excavation, while the horizontal soil movements

*Corresponding author, Professor
E-mail: eng.soomro@gmail.com

ISSN: 2005-307X (Print), 2092-6219 (Online)

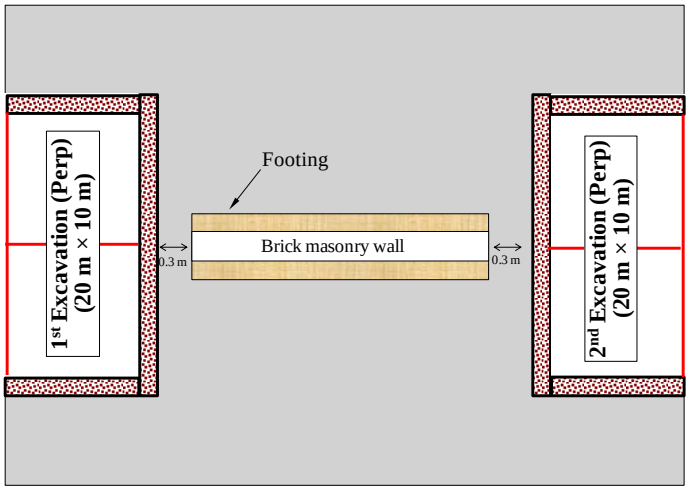

Fig. 1 Plan view of the twin excavations (i.e., perpendicular) adjacent to the existing brick masonry wall

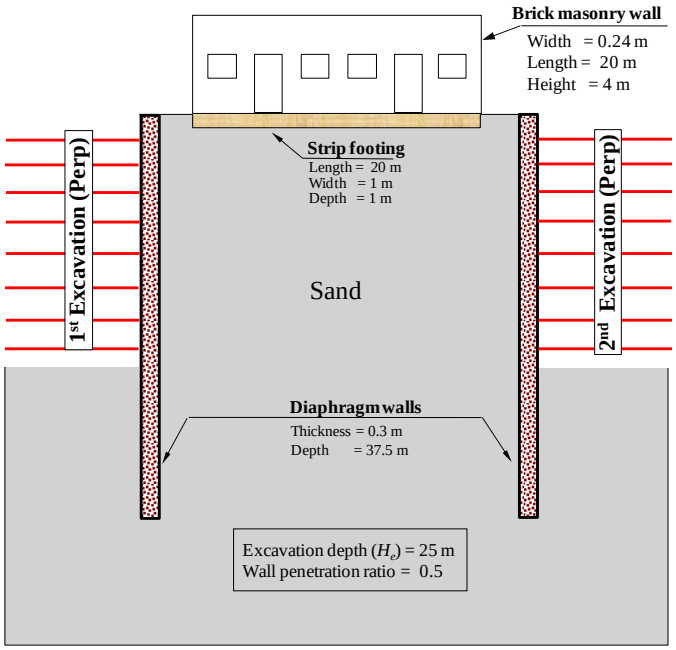

Fig. 2 Elevation view of the configuration of the numerical simulation

were much less in the cases of excavations at both sides. Although extensive work related to stress-release effects on a brick masonry wall has been carried out in the literature. However, most previous studies have focused on the effects of a single excavation on an isolated brick masonry wall.

Owing to non-linear soil behaviour, an excavation can cause a reduction in the stiffness of the ground. Therefore, it is vital to investigate the brick masonry wall responses not only to the first excavation but also subsequent excavation.

To obtain a satisfactory numerical model of the brick masonry wall responses to an adjacent excavation, the analysis needs to take account of the small strain non-linearity of soil. This paper presents a 3D numerical parametric analysis to understand settlement and cracks pattern mechanism in an isolated brick masonry wall due to twin excavations (i.e., perpendicular to the brick masonry wall) in dry sand. In addition, effects of different sand relative destines (i.e., D_r = 30%, 50%, 70% and 90%) on the masonry wall were investigated. Settlement, slope and development of cracks in the wall during twin excavations are reported and discussed.

2. Three-dimensional finite element analysis

2.1 Numerical modelling programme

By using the finite element software Abaqus (2010), three-dimensional numerical analyses were conducted to investigate the effects of twin excavations (i.e., perpendicular to the brick masonry wall) on an adjacent isolated brick masonry wall. Fig. 1(a) shows the twin excavations were carried out on the either sides of the brick masonry wall perpendicularly. To evaluate density effects

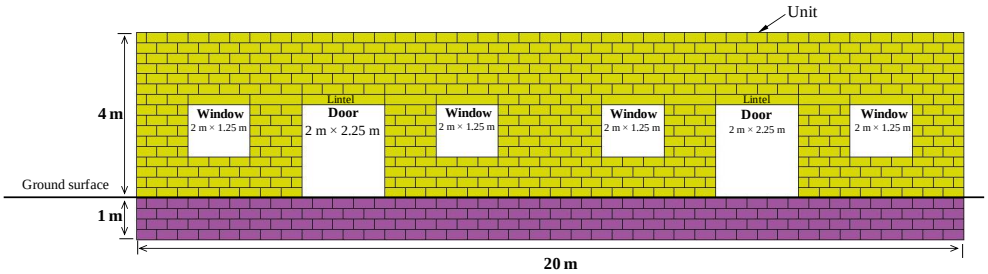

Fig. 3 Details of the isolated brick masonry wall

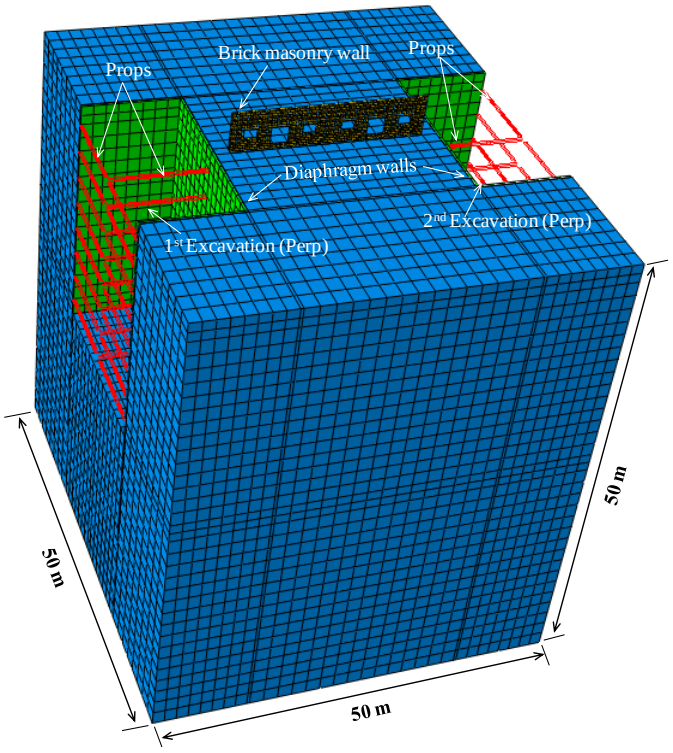

Fig. 4 3D finite element mesh (showing model of the wall, diaphragm walls, and props)

on wall settlements, relative sand densities (D_r) were selected as 30% (i.e., very loose), 50%, 70% (i.e., medium dense) and 90% (very dense). Fig. 2 shows the elevation view of the configuration of the numerical simulation. To simulate long and narrow metro stations, twin excavations with a final excavation depth (H_e) of 25.0 m and a width of 10.0 m were simulated in the numerical analysis, while excavation length was taken as 20 m in each case.

For both excavations, the diaphragm walls had a depth of 37.5 m, having a penetration depth ratio (H_p/H_e) of 0.5, which is a typical penetration depth ratio in engineering practice (Hsiung 2009, Ng *et al.* 2012, Shi *et al.* 2022). Eight levels of props supported the diaphragm walls in both excavations with a vertical and horizontal spacing of 3.0 m and 5 m, respectively. The first level of props was installed at 2.0 m below the ground surface. The props (I-section) are modelled as soft with axial rigidity of 81 × 10^3 kNm (Shi *et al.* 2022, Soomro *et al.* 2022). An existing brick masonry wall 0.4 m thickness and 4.0 m in height was located nearby the basement. The wall is constructed from a brick unit of size 500 mm × 400 mm × 250 mm (Giardina *et al.* 2012, 2013) with two doors (each of size 2 m × 2.25 m) and four windows (each of size 2 m × 1.25 m). The lintels were also provided above all the doors and windows. The wall was founded on a 1 m wide and 1 m deep strip footing. All the details of the isolated brick masonry wall are illustrated in Fig. 3.

2.2 Finite element mesh and boundary conditions

The finite element mesh, consisting of the 3D isolated wall, the foundation, and the soil (incorporating excavation along with diaphragm wall and props), was generated using Abaqus CAE. The depth from the ground surface to the base of the mesh was 50 m, as shown in Fig.4. Eight-noded hexahedral brick elements were used to model the soil, the brick unit, lintels, and the diaphragm wall, while two-noded truss elements were adopted to model the props. The sensitivity of the numerical results with respect to mesh size was explored. It was found that without undermining the

Table 1 Hypoplastic model parameters of sand adopted in this study

Description	Parameter
Effective angle of shearing resistance at critical state: ϕ'_c	31°
Hardness of granulates, h_s	2.6 GPa
Exponent n	0.27
Minimum void ratio at zero pressure, e_{d0}	0.61
Maximum void ratio at zero pressure, e_{c0}	1.10
Critical void ratio at zero pressure, e_{i0}	0.98
Exponent α	0.14
Exponent β	6
Parameter controlling initial shear modulus upon 180° strain path reversal, m_R	11
Parameter controlling initial shear modulus upon 90° strain path reversal, m_T	6
Size of elastic range, R	2×10^{-5}
Parameter controlling degradation rate of stiffness with strain β_r	0.1
Parameter controlling degradation rate of stiffness with strain χ	1.0

stability of analysis, the optimum value of 1.5 mm of elements was chosen. A relatively fine mesh was used near the excavation and the brick masonry wall because large shear strains were expected, and the mesh became coarser further away from the structures. The numerical test shows that further halving current mesh size can only lead to a change of computed results of no more than 0.2%. Roller and pin supports are applied to the vertical sides and the base of the mesh, respectively. Therefore, movements normal to the vertical boundaries and in all directions of the base are restrained. The excavation-induced stress release process was modelled by the "element death" technique widely used in finite element analysis. In this technique, the excavation process was simulated by deactivating soil elements inside the excavation zone. In the meantime, the truss elements representing the props were activated.

2.3 Constitutive model and model parameters used in finite element analysis

Since the stress-strain relationship of soils is highly non-linear even at very small strain and the stiffness of soil depends on the recent stress or strain history of the soil (Atkinson *et al.* 1990, Hong *et al.* 2017), an advanced hypoplastic model was used to simulate the behaviour of sand in this study.

It consists of eight model parameters (ϕ'_c, h_s, n, e_{d0}, e_{c0}, e_{i0}, α and β). The first six parameters (ϕ'_c, h_s, n, e_{d0}, e_{c0}, e_{i0}) of Toyoura sand were calibrated by Herle and Gudehus (1999). The remaining two parameters (α and β) were obtained by curve fitting Maeda and Miura (1999)'s triaxial test results (at large strains). To account for strain-dependency and path-dependency of soil stiffness (at small strains), Niemunis and Herle (1997) further improved the hypoplastic model by incorporating the intergranular strain concept into the model. Five additional parameters (m_R, m_T, R, β_r, and χ) are required.

These five parameters were obtained by fitting the stiffness degradation curves of Toyoura sand obtained from the stress-path triaxial tests carried out by Hong *et al.* (2017). The model parameters were taken from a study by Shi *et al.* (2019). They calibrated and validated all the parameters of the hypoplastic sand model against their centrifuge test results (which was performed to simulate excavation in sand). These parameters are summarized in Table 1.

This study used the micro-modeling technique to model the brick masonry wall (Bolhassani *et al.* 2015). The units were modelled as a linear elastic material with a modulus of elasticity and Poisson's ratio as 6.1 GPa and 0.15, respectively. The density of the brick unit was taken as 1900 kg/m^3. This interaction model provides a way of modelling cohesive connections with negligible thickness interfaces by using the traction-separation constitutive model. This interaction model provides a way of modelling cohesive connections with negligible thickness interfaces by using the traction-separation constitutive model. This surface-based cohesive model is employed to obtain the structural response of masonry along the bed and head joints. The stiffness and damage parameters for the cohesive model parameters are summarised in Table 2 (Nela and Grajçevci 2019). The separation between two brick units was taken as crack width in the finite element analyses. The diaphragm wall-soil interface is modelled as zero thickness by using duplicate nodes. The interface is modelled by the Coulomb friction law, in which the interface friction coefficient (μ) and limiting displacement (γ_{lim}) are required as input parameters. A limiting shear displacement of 5 mm is assumed to achieve full mobilization of the interface friction equal to $\mu\times$p', where p' is the normal effective stress between two contact surfaces and a typical value of μ of 0.35 is used in the analysis (Shi *et al.* 2019). The diaphragm wall and the props were assumed to be linear elastic with Young's modulus of 35 GPa and Poisson's ratio of 0.25. The unit weight of concrete was assumed to be 24 kN/m^3. The lintels were assumed to be made from concrete and were modelled as linearly elastic with Young's modulus of 9 GPa and a Poisson's ratio of 0.2. The coefficient of at-rest earth pressure (K_0=0.5) was estimated based on the effective angle of shearing

Table 2 Cohesive behaviour of joint (Nela and Grajçevci 2019)

Contact behaviour								
Tangential	Normal	Cohesive						
Frictional coefficient		Traction-separation behaviour Stiffness coefficient (N/mm^3)			Damage			
					Initiation (N/mm^2)			Evolution
0.78	Hard contact	K_{nn}	K_{ss}	K_{tt}	Normal	Shear I	Shear II	Plastic displacement (mm)
		360	144	144	0.8	1.0	1.0	2.0

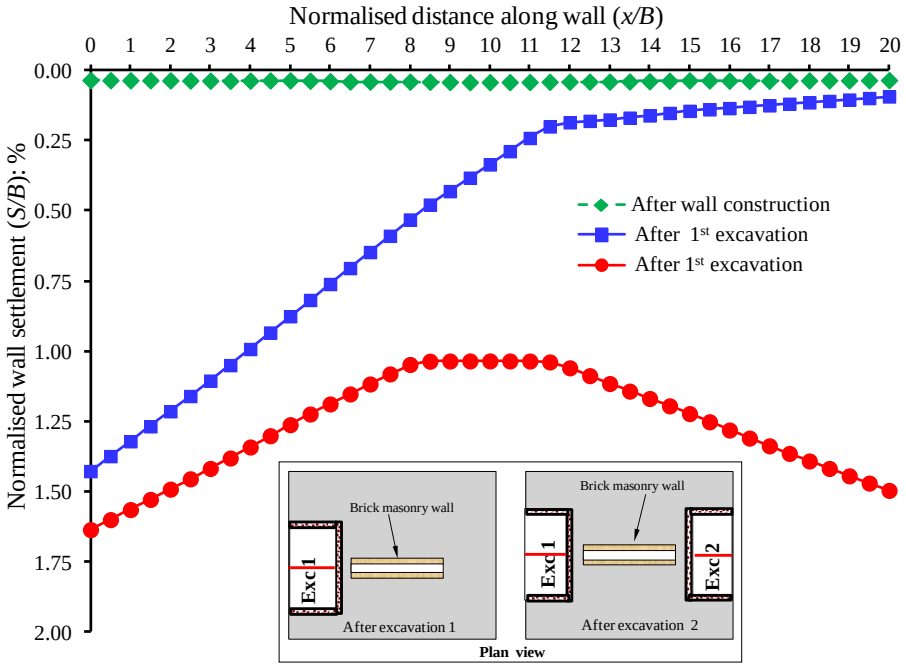

Fig. 5 Settlement of brick masonry wall along the length of footing after first and second excavations

resistance at critical state (ϕ'_c =310) and Jáky (1944)'s equation ($1 - sin\varphi'$).

2.4 Numerical simulation procedure

Each numerical analysis is modelled according to the following steps:

a) Step 1: Initial geostatic stresses were generated in the mesh by applying gravity load and the coefficient of lateral earth pressure of 0.5.
b) Step 2: The footing of the wall was constructed then elements representing brick masonry wall were activated on the footing.
c) Step 3: Activate the brick elements representing the diaphragm wall.
d) Step 4: Staged multi-propped excavation is simulated as described in section 2.1. After excavating to 2 m depth, the first level of props is installed at 2 m below the ground surface.
e) Step 5: Repeat step 4 to excavate the next stages and install props until the last stage of excavation (i.e., H_e= 25 m) is completed.
f) Step 5: Repeat steps 4 and 5 to simulate the second excavation in each case.

3. Interpretation of computed results

3.1 Induced wall settlement due to twin excavations

Fig. 5 shows the settlement (S) along the length of the footing of the brick masonry wall due to the first excavation and the second excavation. The footing settlement (S) is normalized by the width (B) of the footing of the wall. For reference, the footing settlement on completion of the wall (before excavation) is included. As expected, the settlement along the entire footing length is uniform after the construction of the wall (i.e., due to the self-weight of the wall). It can be seen from the figure that the non-uniform settlement was induced in both cases. The induced settlement in the portion of the wall closest to the diaphragm wall (i.e., the first excavation) was larger than that in farthest on completion of the first excavation. The settlement decreased significantly in the portions away from the excavation. This resulted in a differential settlement which caused cracks in the wall. This observation is attributed to a larger stress-release which induced larger shear strain and ground movement near the excavation. This is because larger ground deformation closest to the excavation resulted in a settlement and the development of

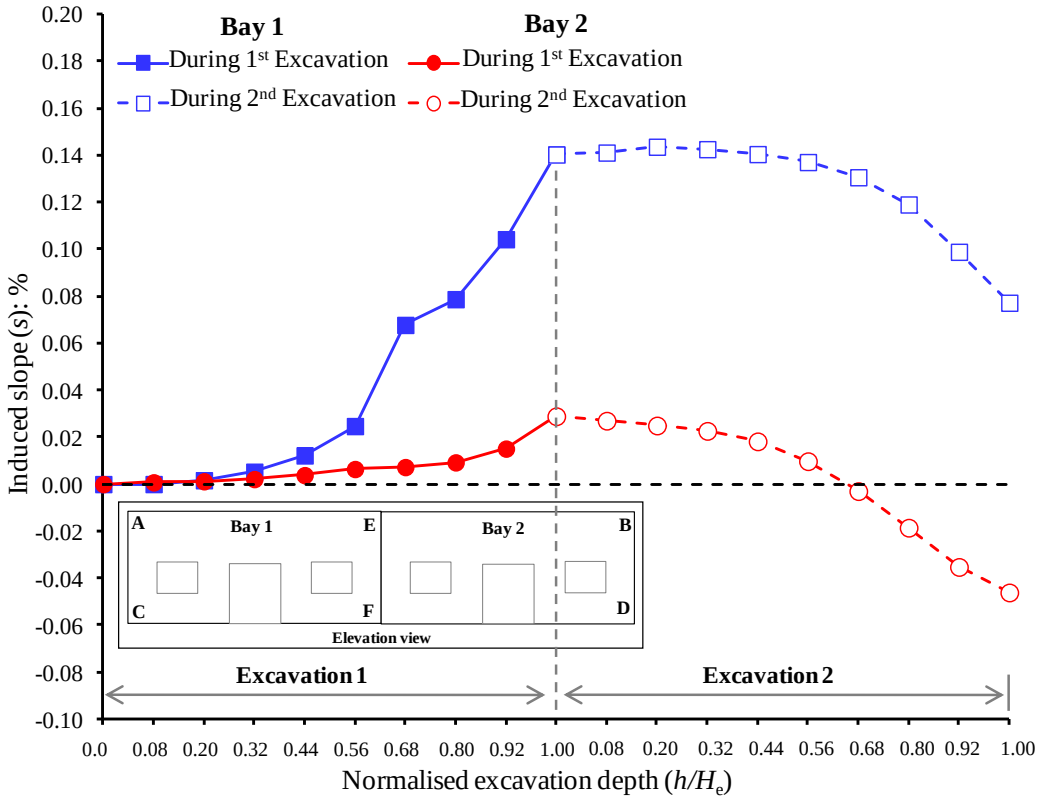

Fig. 6 Induced slope during twin excavations

cracks in the wall. It is further observed that the portion of the wall ($0 \le x/B \le 12$) bends downward, behaving like a cantilever beam. This implies that the upper courses of bricks are subjected to tension which caused the cracks in the wall. The maximum induced settlement at the end of the first excavation was 17.5 mm (1.75B%). The induced settlement further increased in both cases on the completion of twin excavations. Since the location of the brick masonry wall (i.e., perpendicular to both diaphragm walls) was between the twin excavations (see inset in the figure), the portion of the wall closest to the diaphragm wall of the second excavation settled larger than that of farthest portion.

This is because of the larger stress-release, which induced larger shear strain and ground movement near the second excavation. The negligible change in the settlement in the portion of the wall near the first excavation was observed due to the second excavation. This is because the distance between the two excavations is far enough to overlap the excavation-induced shear strain in the ground. Because of the induced differential settlement, the wall bends towards the second excavation. This resulted in the hogging deformation profile of the wall. Consequently, the crack width at the top of the wall increased significantly.

3.2 Induced slope in the wall due to twin excavations

As discussed in the previous section, non-uniform settlement is induced along the length of the brick masonry wall during excavation. This non-uniform settlement is expressed in terms of slope, which is defined as differential settlement at two points of the wall normalized by the horizontal distance between the two settlement points. For convenience, the wall is divided into two bays, namely Bay 1 and Bay 2 (see inset of Fig. 6). Fig. 6 shows the deduced slope (s) of Bay 1 and Bay 2 of the brick masonry wall during the first and the second excavation. As a sign convention, the slope angle measured counter-clockwise from the positive horizontal axis is taken as positive and vice-versa. It can be observed from the figure that the induced slope increased non-linearly in Bay 1 with excavation stages. This is because the vertical side AC is closer to excavation than the other side EF of Bay 1 and hence subjected to larger stress-release and ground deformation, which decreased with distance from the first excavation.

As a result, the induced settlement of point C and lateral movement of point A were larger than that of point F and point E, respectively. This results in the increment of slope in CF of Bay 1 with excavation depth. The increment in the slope of the wall resulted in the widening of the cracks. This is because of the variation of the soil stiffness underneath the footing due to excavation-induced stress relief. Owing to stress release due to deeper excavation stages, the stiffness of the ground at the mid-portion of the excavation degraded significantly. Since Bay 2 is the farthest from the excavation, the induced slope is smaller as compared to that in Bay 1. This observation can be attributed to the ground movement induced due to excavation which is smaller in the portion of Bay 2 as compared to that of Bay 1. Furthermore, most of the part of Bay 2 is located beyond the shear strain zone due to excavation-induced stress release.

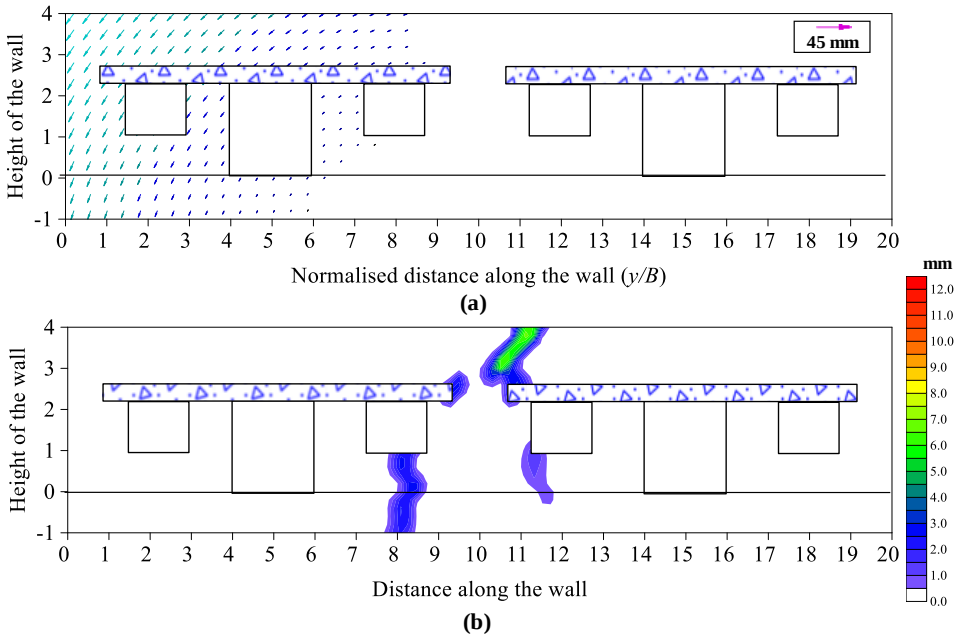

Fig. 7 (a) Displacement vectors of the wall movement and (b) Induced cracks pattern on completion of the first excavation

As the second excavation was commenced, the slope in Bay 1 and Bay 2 reduced with excavation depths. This is because of the location of the second excavation, which is at the opposite side of that the first excavation. Owing to the sagging of the deformed profile of the wall due to twin excavations, the upper bricklayers in the wall were subjected to tensile stresses. Consequently, the crack width at the top of the wall further widened during the second excavation. On completion of twin excavations, final slopes induced in Bay 1 and Bay 2 are +0.08% and -0.05%, respectively.

3.3 Induced displacement and cracks pattern due to twin excavations

As discussed in previous sections, cracks are developed due to settlement and lateral movement of the wall due to twin excavations. To further understand the mechanism of crack development in the wall due to twin excavations, the displacement vectors of wall movement are drawn. Figs. 7(a) and (b) illustrate the induced displacement and crack pattern in the wall due to the first excavation.

The displacement vectors of the wall are larger in the portion of the wall near the first excavation than that in the portion away from the excavation. This is because of the larger ground displacement due to excavation-induced shear strain near the excavation. By inspecting the induced displacement pattern in the wall, the deflection profile of the wall is similar to the cantilever beam subjected to loading. Consequently, the bending of the wall caused tensile stresses at the upper portion of the wall. As a result, each brick unit moves away laterally, causing the crack development in the wall. This mechanism of displacement pattern led to developing cracks in the middle portion of the wall ($8.0 \leq x/B \leq 12.0$) only. The cracks propagate from the face of the lintel at the middle portion of the wall towards the top of the wall (see Fig. 7(b)). Moreover, the cracks developed underneath the window (propagate to the footing of the wall) of Bay 1 near the middle of the wall.

Figs. 8(a) and 8(b) show the induced displacement and cracks pattern in the wall on completion of twin excavations. The displacement vectors show that the movement of the wall occurred on the right side of the wall due to the second excavation. This is because the second excavation was carried out on the right side of the wall, which caused higher stress release closest to the second excavation. The portion of the wall closest to the diaphragm wall (i.e., the second excavation) settled larger than that of the farthest portion. This is because of the larger stress-release, which induced larger shear strain and ground movement near the second excavation. By inspecting the induced displacement pattern in the wall, the hogging deformation profile was induced in the wall on completion of the twin excavations. Consequently, the width of cracks at the top of the wall increased significantly. However, the pattern of the cracks remained the same as that due to the first excavation.

3.4 Crack width during twin excavation

To quantify the crack width during twin excavations, two critical locations were selected at the top and footing of the wall (see inset in Fig. 9). Fig. 9 shows the development of the width of the cracks at the selected locations during twin excavation. The crack development is consistent with the induced settlement and slope in the wall. The width of all the cracks grows non-linearly with excavation depth during twin excavations at both locations. The maximum crack width (i.e., 7 mm) was developed at the top of the wall on completion of excavation. This is because the wall deformation profile (see Fig. 5) exhibits the behaviour of a cantilever beam with a maximum deflection at the corner

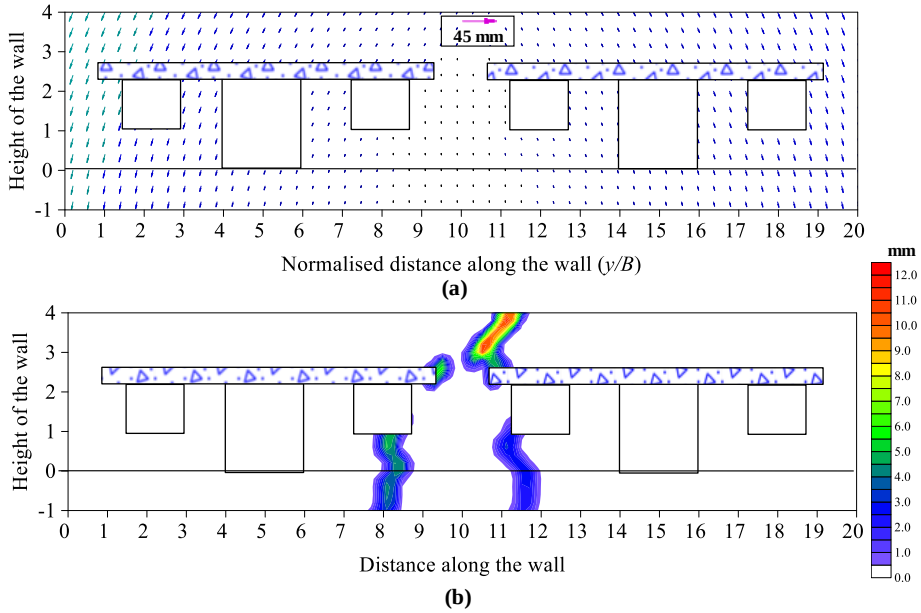

Fig. 8 (a) Displacement vectors of the wall movement and (b) Induced crack patterns on completion of the twin excavations

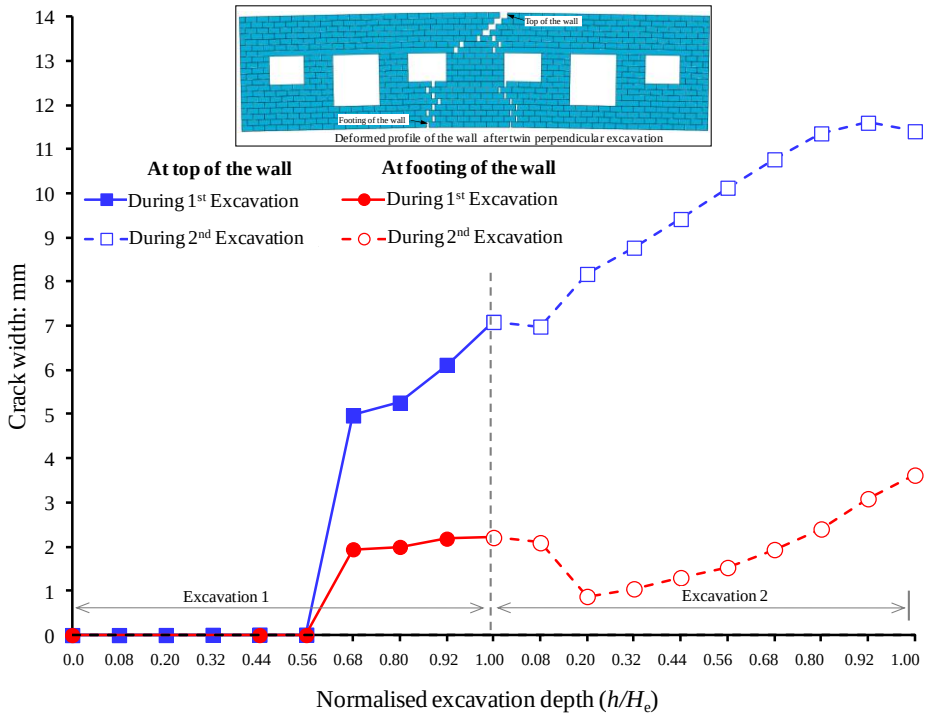

Fig. 9 Development of crack width in the wall during twin excavations

near the excavation. This results in the development of tensile stresses at the upper portion of the wall. Consequently, each brick unit moves away laterally, which caused the development of the cracks in the upper courses of the wall. Each brick unit is bonded with mortar with brittle behaviour. The mortar sustained the pull of brick till the excavation stage of h/H_e=0.56. However, as excavation goes deeper, the rate of induced settlement slope and lateral wall movement increases caused the development of cracks on the wall.

The crack width developed in the foundation and the lower portion of the wall is less than that in the upper layers of the wall. Due to the second excavation, the rate of crack growth increased in the wall. This is because of the location of the second excavation, which is at the opposite side of that the first excavation. Owing to the sagging deformed profile of the wall due to twin excavations, the upper bricklayers in the wall were subjected to tensile stresses. Consequently, the crack width at the top of the wall and footing further widened during the second excavation. The

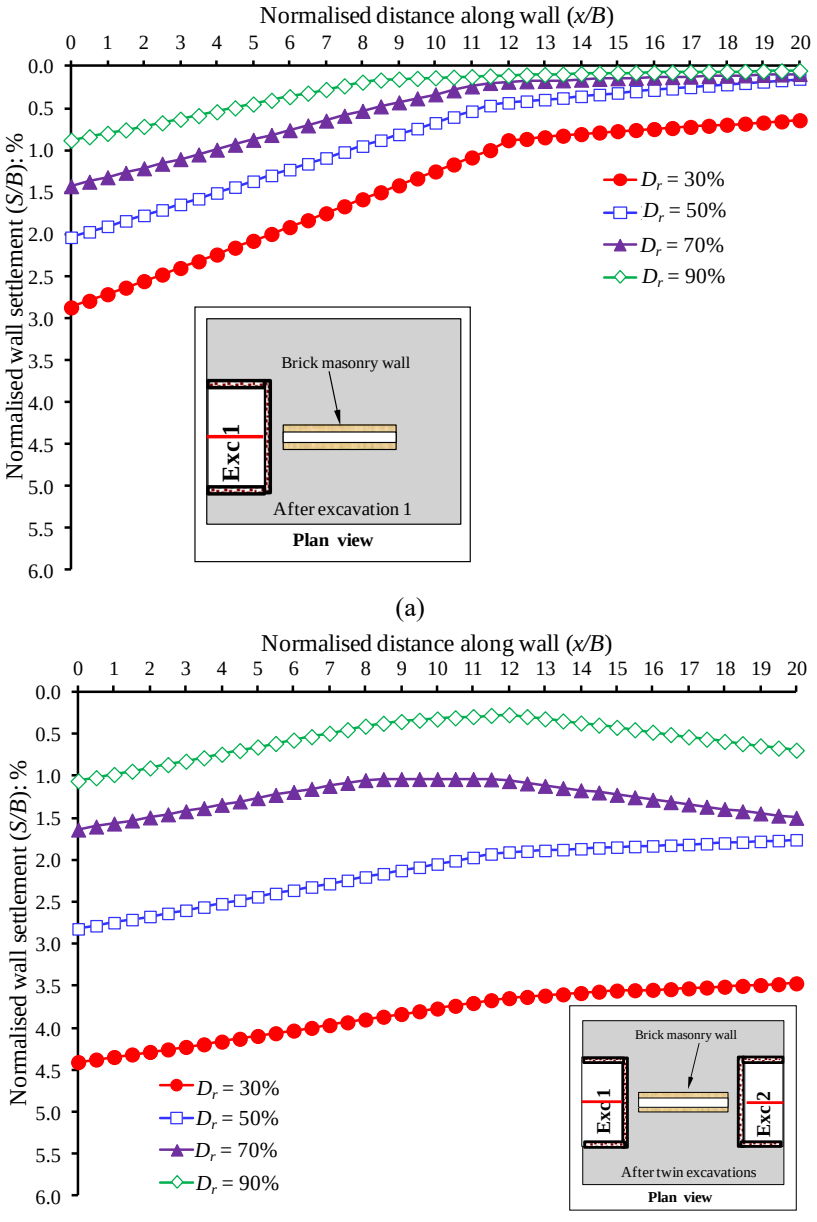

Fig. 10 Effects of sand density of on induced settlement of the brick masonry wall on completion of (a) first excavation and (b) twin excavations

crack widths of 12 and 4 mm were developed on completion of twin excavations at the top and the footing the wall, respectively.

3.4 Effects of density of ground (sand)

3.4.1 Induced footing settlement

Fig. 10(a) shows the influence of sand relative density (i.e. D_r = 30%, 50%, 70% and 90%) on the settlement along the footing on completion of first excavation. It can be seen from the figure that the induced maximum footing settlement decreases almost linearly with increasing sand relative density.

Moreover, the influence zone of the induced settlement increases in loose (i.e., D_r = 30%) sand than that in very dense sand (D_r = 90%). On completion of the excavation (h/H_e=1.0), the footing settlement in loose sand (D_r=30%) and dense sand (D_r=90%) are 2.9B% and 0.9B%, respectively. The settlement of the footing was reduced by 70%. This is because loose sand has a smaller shear modulus. Due to excavation-induced stress relief, large soil movements are induced in loose sand (discussed in section 3.4.3), causing larger footing settlement. Consequently, the larger cracks are induced in the façade constructed on loose sand (discussed in section 3.4.2). Since shallow excavations induce smaller stress relief, the effects of the relative density of sand on footing settlement is less significant than that of deep excavations. Similar effects of relative density of sand were identified on the footing settlement due to subsequent excavation which is located on the other side of

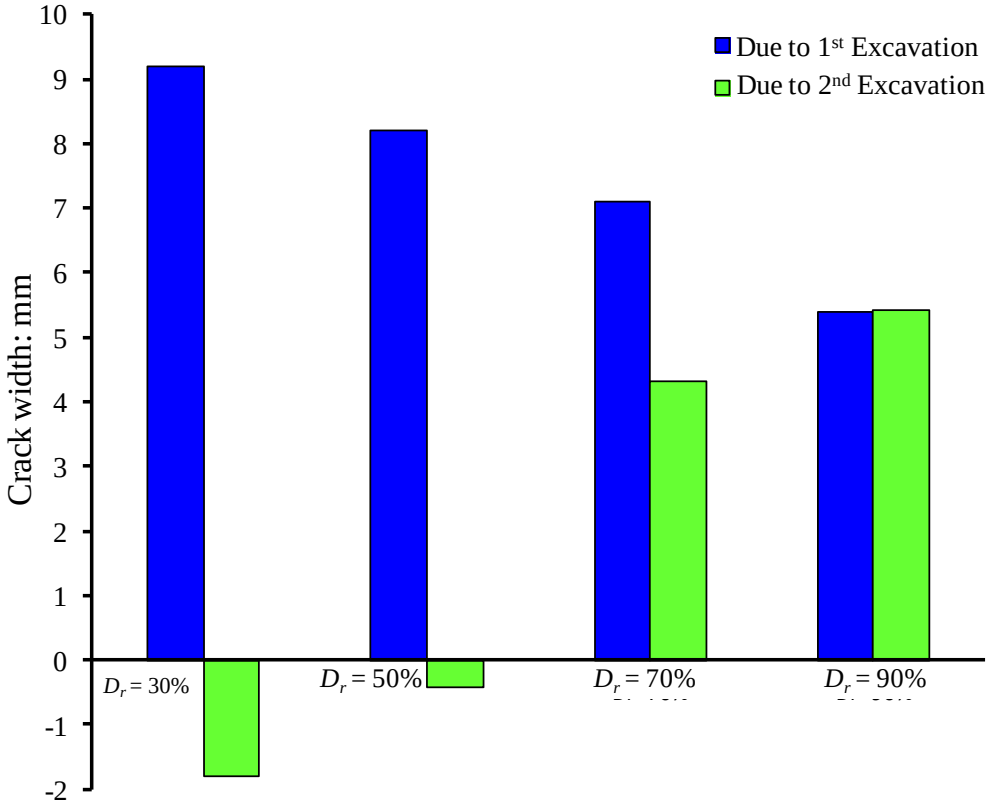

Fig. 11 Development of crack width in the wall during twin excavations

the masonry wall, as shown in Fig. 10(b). The induced settlement was smaller in very dense sand that in very loose sand. The hogging deformation profile of the masonry wall has been identified from induced settlement of the masonry wall in medium to dense sand (i.e., 70% and 90%). This is because of the induced shear strain and ground movement are localised to the excavations (discussed in section 3.4.2).

This results in different settlement of the wall. Consequently, the crack width at the top of the wall due to second excavation increased significantly (discussed in section 3.4.2). On the contrary, the induced footing settlement is uniform in loose to very loose sand (i.e., 50% and 30%). This can ascribed to the induced ground movement and shear strain due to second excavation. The influence zone of the ground movement and shear stain due to twin excavations overlap each other which results in uniform settlement in loose to very loose sand as compared to that in in medium to dense sand. This results in the reduction of crack width on the top of the masonry wall (discussed in section 3.4.2).

3.4.2 Induced cracks in the wall

To investigate the consequences of excavation-induced footing settlement on the wall in different relative densities of sand, the largest crack location which is top of the masonry wall was selected. Fig. 11 illustrates the width of crack on the top of the masonry wall due to first and second excavation in ground with different relative density (i.e., D_r = 30%, 50%, 70% and 90%). It can be seen that the crack width in the wall decreases as the sand density increases due to first excavation. This is because of larger settlement in very loose sand than that in very dense sand near the first excavation. This led to induced differential settlement of the wall which resulted in the hogging deformation profile of the wall (see Fig. 10(a)). Consequently, the largest cracks were developed in top of the wall in very loose sand than that in very dense sand. In contrast, the crack width decreases on the top of the wall on completion of the second excavation in very loose to loose sand (D_r = 30%, 50%). Whilst the second excavation in medium to very dense sand (D_r = 70% and 90%) caused to increase the crack width on the top of the wall. This can be attributed to the induced ground movement and shear strain due to second excavation. The influence zone of the ground movement and shear stain due to twin excavations overlap each other which results in uniform settlement in loose to very loose sand as compared to that in in medium to dense sand. This results in the reduction of crack width on the top of the masonry wall (discussed in section 3.4.3). On the other hand, the induced shear strain and ground movement are localised to the excavations in medium to very dense sand (discussed in section 3.4.3). This results in different settlement of the wall. Consequently, the crack width at the top of the wall due to second excavation increased significantly. This clearly suggests that the relative density of sand has substantial effects on the responses of the wall due to twin excavation-induced stress relief. The final crack widths of 7.4, 7.8, 11.4 and 10.8 mm were computed on completion of twin excavations in ground of D_r = 30%, 50%, 70% and 90%, respectively.

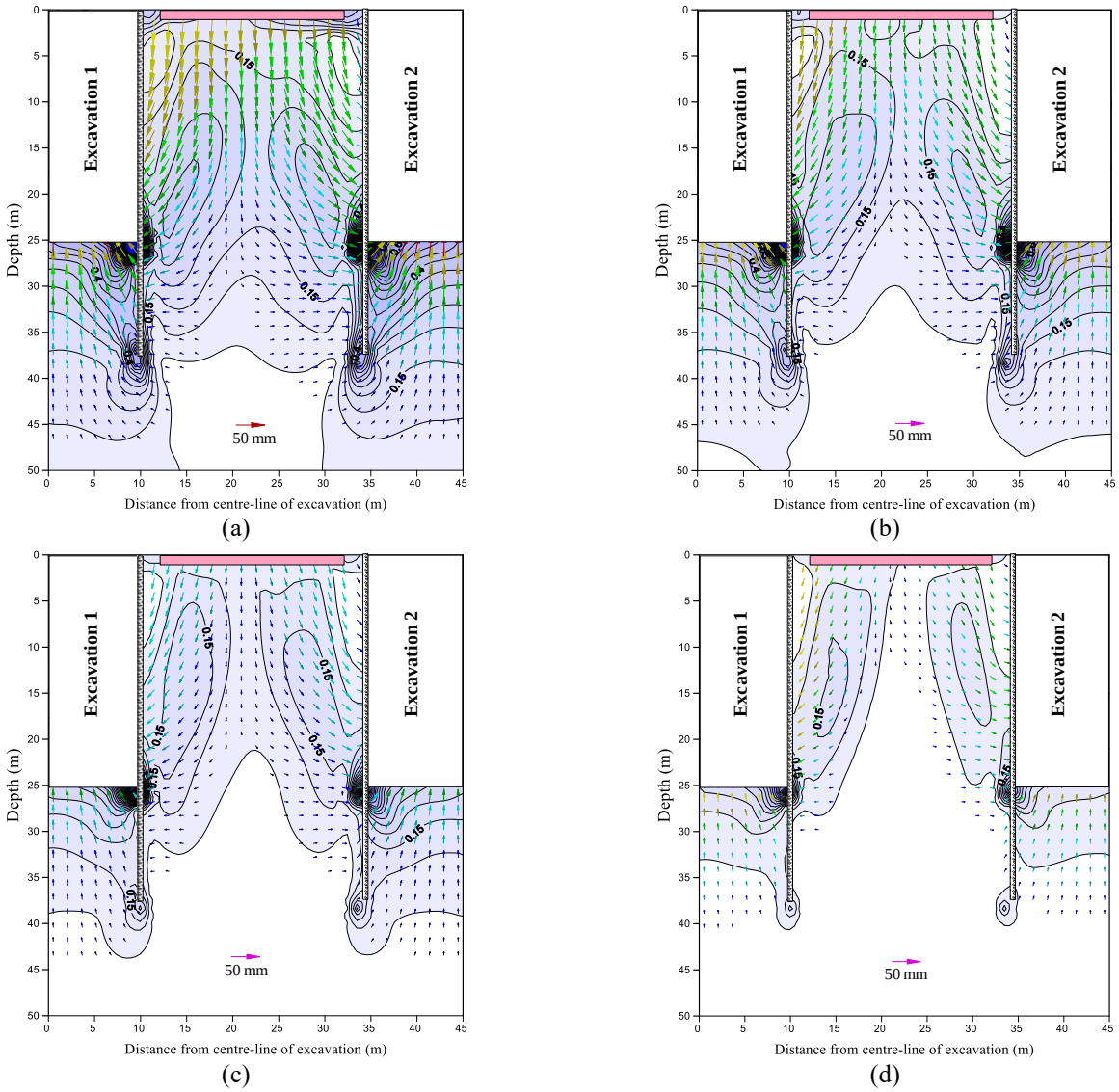

Fig. 12 Effects of the sand relative density on the ground movements and shear strain (a) D_r = 30%; (b) D_r = 50%; (c) D_r = 70% and (d) D_r = 90%

3.4.3 Induced soil movement and shear strain in the ground

Figs. 12(a)-12(d) show the soil movement on completion of twin excavations in the ground with different sand densities of D_r = 30%, 50%, 70% and 90%, respectively. In addition, computed incremental shear strain the excavation induced stress release is also superimposed in the figure. It can be seen from the figure that downward ground movement is induced behind the diaphragm wall in all the cases. However, the heave in the formation level was induced at excavation side. The deep-seated horizontal soil movements indicate the "bulging" profiles of the wall deformation. The soil movement in loose ground (i.e., D_r=30%) is larger than that in denser grounds. This is because of lower shear modulus of loose sand. The horizontal influence zone is larger when the sand density is lower (ranging from 1.6 to 0.6H_e for D_r=30% and 90%, respectively). Moreover, the influence zone of the ground movement and shear stain due to twin excavations overlap each other which results in uniform settlement in loose to very loose sand (i.e., D_r = 30%, 50%) as compared to that in in medium to dense sand. As a consequence of this, in the reduction of crack width on the top of the masonry wall (see Fig. 11). When twin excavations were carried out in dense to very dense sand (D_r = 70%, 90%), the induced shear strain and ground movement are localised to each excavation.

Hence, the portion of the masonry wall close to each excavation settled, resulting in the hogging deformation profile of the wall. Consequently, the crack width at the top of the wall due to second excavation increased significantly (see Fig. 11). The different mechanism of induced ground movement and shear strain contours due to twin excavations in the ground with different sand densities clearly suggests that the relative density of sand has substantial effects on the responses of the wall due to twin excavation-induced stress relief.

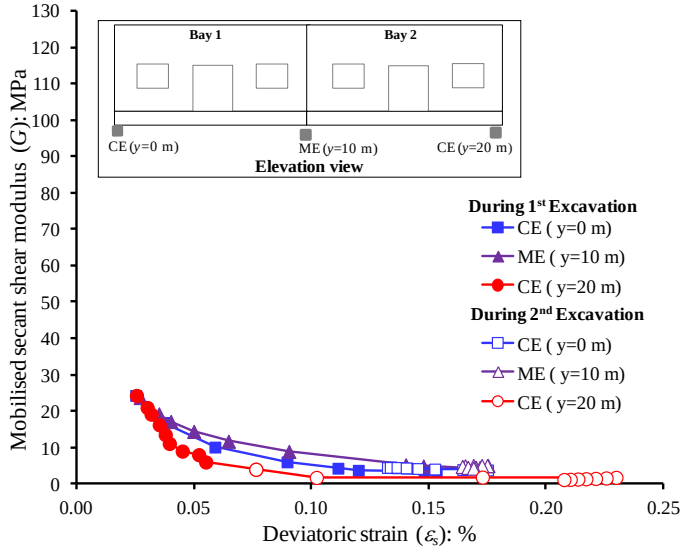

(a)

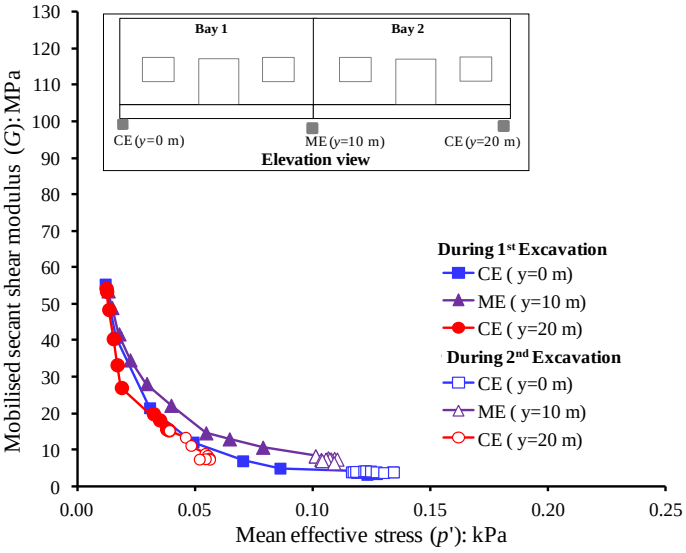

(b)

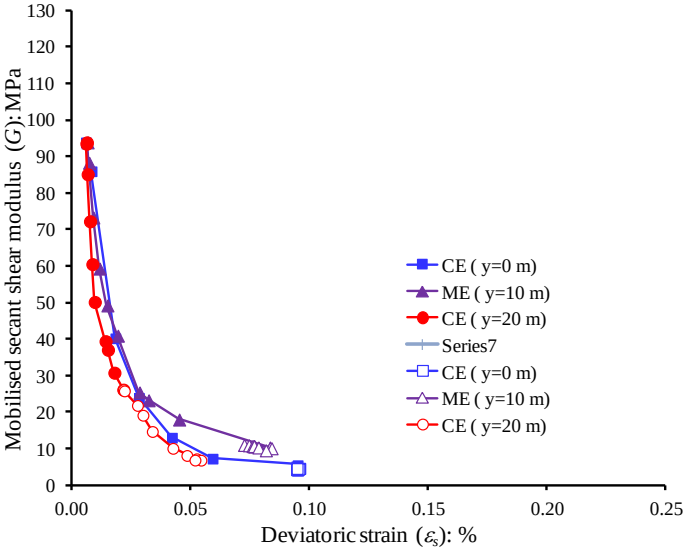

(c)

Fig. 13 Changes in shear stiffness during twin excavations (a) D_r = 30%, (b) D_r = 50%, (c) D_r = 70% and (d) D_r = 90%

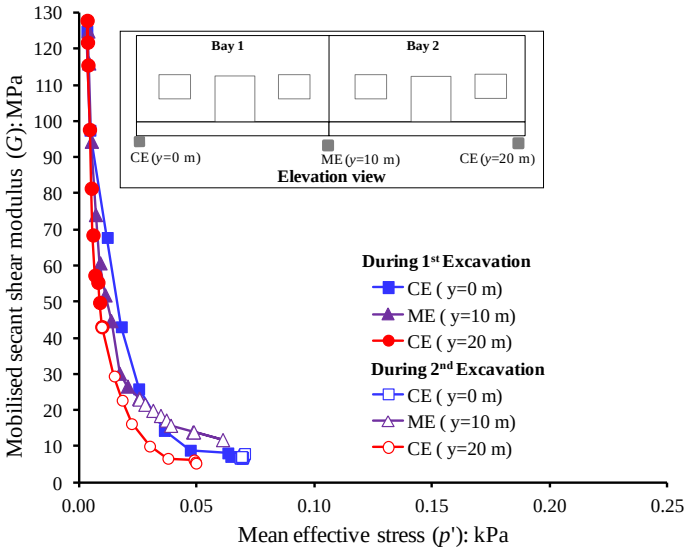

(d)

Fig. 13 Continued-

3.4.4 Induced ground stiffness during excavation

To substantiate discussion from the previous section, mobilized secant shear stiffness of soil elements underneath the wall footing is interpreted in this section. The mobilized secant shear modulus (G_m) values were calculated from the following equations

$$G_m = q/3\varepsilon_s \tag{1}$$

$$q = \frac{1}{\sqrt{2}}\sqrt{[(\sigma_1-\sigma_2)^2+(\sigma_2-\sigma_3)^2+(\sigma_3-\sigma_1)^2]} \tag{2}$$

$$\varepsilon_s = \sqrt{\frac{2}{9}[(\varepsilon_1-\varepsilon_2)^2+(\varepsilon_2-\varepsilon_3)^2+(\varepsilon_3-\varepsilon_1)^2]} \tag{3}$$

where q and ε_s are the computed deviatoric stress and strain, respectively. σ_i and ε_i are the principal stresses and principal strains, respectively.

Figs. 11(a)-11(d) show the variation of the mobilized secant shear modulus of soil elements (see inset in the figure) underneath the footing during twin excavations in the in the ground with different sand densities of D_r = 30%, 50%, 70% and 90%, respectively.

It can be seen from the figure that mobilized shear modulus is higher in dense sand. This is because under the same mean effective stress, the initial stiffness is higher. In addition, less deviatoric strain was induced in denser sand and thus low stiffness degradation occurred. After the first excavation, significant degradation of the stiffness of the three selected elements occurred. Comparing the stiffness degradation of the element CE (y=0 m), the stiffness degradation of the elements ME (y=10 m) and CE (y=20 m) is small. This is because the element CE (y=0 m) is near to the first excavation and subjected to higher excavation-induced stress release. As a result, the settlement of the portion of the brick masonry wall closer to the excavation is higher than that in the farthest (see Fig. 10). When the second excavation was carried out, the stiffness of the element CE (y=20 m, which is closest to the second excavation) further degrade causing the settlement of the wall portion near to the second excavation. The shear stiffness degradation of loose sand (i.e., Dr=30%) is larger during excavation because of larger induced deviatoric strain. This resulted in the larger footing settlement in loose sand (see Fig. 10).

4. Conclusions

This paper presents a 3D numerical parametric analysis to understand settlement and cracks pattern mechanism in an isolated brick masonry wall due to twin excavations (i.e., perpendicular to the brick masonry wall) in dry sand. In addition, effects of different sand relative destines (i.e., D_r = 30%, 50%, 70% and 90%) on the masonry wall were investigated. Settlement, slope and development of cracks in the wall during twin excavations are reported and discussed. To accurately capture the excavation-induced ground deformation, path- and strain-dependent soil stiffness at small strains were taken into account in each numerical analysis by adopting an advanced hypoplastic sand model coupled with the inter-granular strain formulation. Based on the computed results, the following conclusions can be drawn:

(a) The induced settlement in the portion of the wall closest to the diaphragm walls of both excavations was larger than that in farthest on completion of the first and the second excavations. The settlement decreased significantly in the portions away from the excavations. This is because of the larger stress-release, which induced larger shear strain and ground movement near each excavation. Because of the induced differential settlement, the wall bends towards each excavation. This resulted in the hogging deformation profile of the wall. Consequently, the width of the crack at the top of the wall increased significantly.

(b) The rate of crack growth increased in the wall due to the second excavation. This is because of the location of the second excavation, which is at the opposite side of that of the first excavation. Owing to the hogging of the brick masonry wall due to the twin excavations, the upper bricklayers in the wall were subjected to tensile stresses. Consequently, the crack width at the top of the wall during the second excavation. The crack width of 12 and 4 mm were developed on completion of twin excavations at the top and footing of the wall, respectively.
(c) By increasing the relative density from 30% to 90%, the induced footing settlement decreases significantly. The hogging deformation profile of the masonry wall has been identified from induced settlement of the masonry wall in medium to dense sand (i.e. 70% and 90%). On the contrary, the induced footing settlement is uniform in loose to very loose sand (i.e., 50% and 30%).
(d) On completion of the second excavation in very loose to loose sand (D_r = 30%, 50%), the crack width decreases on the top of the wall. Whilst the second excavation in medium to very dense sand (D_r = 70% and 90%) caused to increase the crack width on the top of the wall. This can be attributed to the induced ground movement and shear strain due to second excavation. The influence zone of the ground movement and shear stain due to twin excavations overlap each other which results in uniform settlement in loose to very loose sand as compared to that in in medium to dense sand. On the other hand, the induced shear strain and ground movement are localised to the excavations in medium to very dense sand.

It should be noted that the computed results reported in this paper should be treated with caution since they may be specific to the particular soil type and isolated wall type adopted.

Acknowledgments

The authors would like to acknowledge the financial support provided by China University of Mining and Technology, Xuzhou, China.

Conflicts of Interest

The authors declare that they have no conflicts of interest.

References

Abdulla, K.F., Cunningham, L.S. and Gillie, M. (2017), "Simulating masonry wall behaviour using a simplified micro-model approach", *Eng. Struct.*, **151**, 349-365. https://doi.org/10.1016/j.engstruct.2017.08.021

Atkinson, J.H., Richardson, D. and Stallebrass, S.E. (1990), "Effect of recent stress history on the stiffness of over consolidated soil", *Géotechnique*, **40**(4), 531-540. https://doi.org/10.1680/geot.1990.40.4.531.

Basmaji, B., Deck, O. and Al Heib, M. (2019), "Analytical model to predict building deflections induced by ground movements", *Eur. J. Environ. Civil Eng.*, **23**(3), 409-431. https://doi.org/10.1080/19648189.2017.1282382.

Bejarano-Urrego, L., Verstrynge, E., Giardina, G. and Van Balen, K. (2018), "Crack growth in masonry: Numerical analysis and sensitivity study for discrete and smeared crack modelling", *Eng. Struct.*, **165**, 471-485. https://doi.org/10.1016/j.engstruct.2018.03.030.

Bolhassani, M., Hamid, A.A., Lau, A.C. and Moon, F. (2015), "Simplified micro modeling of partially grouted masonry assemblages", *Constr. Build. Mater.*, **83**, 159-173. https://doi.org/10.1016/j.conbuildmat. 2015.03.021.

Chen, P., Wang, W.D. and Ding, J.F. (2013), "Design and application of synchronous construction of two neighboring deep excavations", *Chinese J. Geotech. Eng.*, **35**(2), 555-558.

Dong, Y., Burd, H.J. and Houlsby, G.T. (2017), "Finite element study of deep excavation construction processes", *Soils Found.*, **57**(6), 965-979. https://doi.org/10.1016/j.sandf.2017.08.024.

Ding, Z., Wei, X.J. and Wei, G. (2017), "Prediction methods on tunnel-excavation induced surface settlement around adjacent building", *Geomech. Eng.*, **12**(2), 185-195. https://doi.org/10.12989/gae.2017.12.2.185.

El Sawwaf, M. and Nazir, A.K. (2012), "The effect of deep excavation-induced lateral soil movements on the behavior of strip footing supported on reinforced sand", *J. Adv. Res.*, **3**(4), 337-344. https://doi.org/10.1016/j.jare.2011.11.001.

Ghahreman, B (2004), "Analysis of ground and building response around deep excavation in sand", Ph. D. Thesis, Department of civil eng., University of Illinois

Giardina, G., Hendriks, M.A. and Rots, J.G. (2010), "Numerical analysis of tunnelling effects on masonry buildings: the influence of tunnel location on damage assessment", *Adv. Mater. Res.*, **133**, 289-294. https://doi.org/10.4028/www.scientific.net/AMR.133-134.289.

Giardina, G., Marini, A., Hendriks, M.A., Rots, J.G., Rizzardini, F. and Giuriani, E. (2012), "Experimental analysis of a masonry façade subject to tunnelling-induced settlement", *Eng. Struct.*, **45**, 421-434. https://doi.org/10.1016/j.engstruct.2012.06.042.

Giardina, G., Van de Graaf, A.V., Hendriks, M.A., Rots, J.G. and Marini, A. (2013), "Numerical analysis of a masonry façade subject to tunnelling-induced settlements", *Eng. Struct.*, **54**, 234-247. https://doi.org/10.1016/j.engstruct.2013.03.055.

Giardina, G., Hendriks, M.A. and Rots, J.G. (2015), "Sensitivity study on tunnelling induced damage to a masonry façade", *Eng. Struct.*, **89**, 111-129. https://doi.org/10.1016/j.engstruct.2013.03.055.

Gudehus, G. (1996), "A comprehensive constitutive equation for granular materials", *Soils Found.*, **36**(1), 1-12. https://doi.org/10.3208/sandf.36.1.

Halim, D. and Wong, K.S. (2012), "Prediction of frame structure damage resulting from deep excavation", *J. Geotech. Geoenviron. Eng.*, **138**(12), 1530-1536. DOI:10.1061/(asce)gt.1943-5606.0000682.

Hashemi, H., Naeimifar, I., Uromeihy, A. and Yasrobi, S. (2015), "Evaluation of rock nail wall performance in jointed rock using numerical method", *Geotech. Geol. Eng.*, **33**(3), 593-607. https://doi.org/10.1007/s10706-015-9842-3.

Herle, I. and Gudehus, G. (1999), "Determination of parameters of a hypoplastic constitutive model from properties of grain assemblies", *Mechanics of Cohesive-frictional Materials: An International Journal on Experiments, Modelling and Computation of Materials and Structures*, **4**(5), 461-486. https://doi.org/10.1002/(sici)10991484(199909)4:5%3C461::aid-cfm71%3E3.0.co;2-p.

Hibbitt, Karlsson, Sorensen, (2010), Abaqus user's manual, version 6.10.2. Hibbitt, Karlsson & Sorensen Inc;, Providence, RI, USA.

Hong, Y. and Ng, C.W. (2013), "Base stability of multi-propped excavations in soft clay subjected to hydraulic uplift", *Can. Geotech. J.*, **50**(2), 153-164. https://doi.org/10.1139/cgj-2012-0170

Hong, Y., Koo, C.H., Zhou, C., Ng, C.W. and Wang, L.Z. (2017), "Small strain path-dependent stiffness of Toyoura sand: Laboratory measurement and numerical implementation", *Int. J. Geomech.*, **17**(1), 04016036. https://doi.org/10.1061/(asce)gm.1943-5622.0000664.

Hsiung, B.C.B. (2009), "A case study on the behaviour of a deep excavation in sand", *Comput. Geotech.*, **36**(4), 665-675. https://doi.org/10.1016/j.compgeo.2008.10.003.

Jamil, I. and Ahmad, I. (2019), "Bending moments in raft of a piled raft system using Winkler analysis", *Geomech. Eng.*, **18**(1), 41-48. https://doi.org/10.12989/gae.2019.18.1.041.

Jáky J. (1944), "The coefficient of earth pressure at rest", *J. Soc. Hungarian Arch. Eng*., 355-358. [in Hungarian].

Karira, H., Kumar, A., Ali, T.H., Mangnejo, D.A. and Mangi, N. (2022), "A parametric study of settlement and load transfer mechanism of piled raft due to adjacent excavation using 3D finite element analysis", *Geomech. Eng.*, **30**(2), 169-185. https://doi.org/10.12989/gae.2022.30.2.169.

Lasciarrea, W.G., Amorosi, A., Boldini, D., de Felice, G. and Malena, M. (2019), "Jointed masonry model: A constitutive law for 3D soil-structure interaction analysis", *Eng. Struct.*, **201**, 109803. https://doi.org/10.1016/j.engstruct.2019.109803.

Lin, H.D., Truong, H.M., Dang, H.P. and Chen, C.C. (2014), "Assessment of 3D excavation and adjacent building's reponses with consideration of excavation-structure interaction", *Tunn. Undergr. Constr.*, 256-265. https://doi.org/10.1061/9780784413449.026.

Lee, S.W. (2019), "Experimental study on effect of underground excavation distance on the behavior of retaining wall", *Geomech. Eng.*, **17**(5), 413-420. https://doi.org/10.12989/gae.2019.17.5.413

Maeda, K. and Miura, K. (1999), "Relative density dependency of mechanical properties of sands", *Soils Found*., **39**(1), 69-79. https://doi.org/10.3208/sandf.39.69.

Mu, L., Huang, M., Roodi, G.H. and Shi, Z. (2021), "Allowable wall deflection of braced excavation adjacent to pile-supported buildings", *Geomech. Eng*., **26**(2), 161-173. https://doi.org/10.12989/gae.2021.26.2.161.

Minh TH (2013), "Study of excavation behavior and adjacent building response with 3D simulation", *Doctoral dissertation, Master dissertation, National Taiwan University of Science and Technology*.

Naeimifar, I., Yasrobi, S., Golshani, A.A. and Joneidi, M. (2021), "Damage estimation in masonry buildings based on excavation-induced ground movements", *Geotech. Geol. Eng.*, 1-21. https://doi.org/10.1007/s10706-021-01757-4.

Nela, B. and Grajçevci, F. (2019), "Numerical approach: fem testing of masonry specimens with different bond configurations of units", *Proceedings of the Congresso de Métodos Numéricos em Engenharia1-3 julho 2019*, Guimarães, Portugal Universidade do Minho, 1-17.

Niemunis, A. and Herle, I. (1997), "Hypoplastic model for cohesionless soils with elastic strain range", *Mechanics of Cohesive-frictional Materials: An International Journal on Experiments, Modelling and Computation of Materials and Structures*, **2**(4), 279-299. https://doi.org/10.1002/(SICI)1099-1484(199710)2:4<279::AID-CFM29>3.0.CO;2-8.

Ng, C.W.W., Hong, Y., Liu, G.B. and Liu, T. (2012), "Ground deformations and soil–structure interaction of a multi-propped excavation in Shanghai soft clays", *Géotechnique*, **62**(10), 907-921. https://doi.org/10:1680/geot.10.P.072.

Orazalin, Z.Y., Whittle, A.J. and Olsen, M.B. (2015), "Three-dimensional analyses of excavation support system for the Stata Center basement on the MIT campus", *J. Geotech. Geoenviron. Eng.*, **141**(7), 05015001. https://doi.org/10.1061/(ASCE)GT.1943-5606.0001326.

Ou, C.Y., Liao, J.T. and Cheng, W.L. (2000), "Building response and ground movements induced by a deep excavation", *Geotechnique*, **50**(3), 209-220. https://doi.org/10.1680/geot.2000.50.3.209.

Qian, J., Tong, Y., Mu, L., Lu, Q. and Zhao, H. (2020), "A displacement controlled method for evaluating ground settlement induced by excavation in clay", *Geomech. Eng*., **20**(4), 275-285. https://doi.org/10.12989/gae.2020.20.4.275.

Ruan, H.T., Zhao, J.H., Huang, W.D. and Liu, L. (2010), "Design and analysis of concurrent excavation of adjacent deep foundation pits", *Chinese J. Geotech.Eng.*, **32**, 249-254.

Schuster, M., Kung, G.T.C., Juang, C.H. and Hashash, Y.M. (2009), "Simplified model for evaluating damage potential of buildings adjacent to a braced excavation", *J. Geotech. Geoenviron. Eng.*, **135**(12), 1823-1835.

Shen, J. (2012), "Analyses and countermeasures on interaction among large-scale group excavation projects", *Chinese J. Geotech. Eng.*, **34**, 272-276

Shi, J., Liu, G., Huang, P. and Ng, C.W.W. (2015), "Interaction between a large-scale triangular excavation and adjacent structures in Shanghai soft clay", *Tunn. Undergr. Sp. Tech.*, **50**, 282-295. https://doi.org/10.1016/j.tust.2015.07.013.

Shi, J., Fu, Z. and Guo, W. (2019a), "Investigation of geometric effects on three-dimensional tunnel deformation mechanisms due to basement excavation", *Comput. Geotech.*, **106**, 108-116. https://doi.org/10.1016/j.compgeo.2018.10.019.

Shi, J., Wei, J., Ng, C.W. and Lu, H. (2019b), "Stress transfer mechanisms and settlement of a floating pile due to adjacent multi-propped deep excavation in dry sand", *Comput. Geotech.*, **116**, 103216. https://doi.org/10.1016/j.compgeo.2019.103216.

Shi, J., Ding, C., Ng, C.W.W., Lu, H. and Chen, L. (2020), "Effects of overconsolidation ratio on tunnel responses due to overlying basement excavation in clay", *Tunn. Undergr. Sp. Tech.*, **97**, 103247. https://doi.org/10.1016/j.tust.2019.103247.

Son, M. and Cording, E.J. (2005), "Estimation of building damage due to excavation-induced ground movements", *J. Geotech. Geoenviron. Eng.*, **131**(2), 162-177. https://doi.org/10.1061/(ASCE)1090-0241(2005)131:2(162).

Son, M. and Cording, E.J. (2008), "Numerical model tests of building response to excavation-induced ground movements", *Can. Geotech. J.*, **45**(11), 1611-1621. https://doi.org/10.1139/T08-074.

Son, M. and Cording, E.J. (2011), "Responses of buildings with different structural types to excavation-induced ground settlements", *J. Geotech. Geoenviron. Eng.*, **137**(4), 323-333. https://doi.org/10.1061/(ASCE)GT.1943-5606.0000448.

Soomro, M.A., Mangi, N., Memon, A.H. and Mangnejo, D.A. (2022), "Responses of high-rise building resting on piled raft to adjacent tunnel at different depths relative to piles", *Geomech. Eng.*, **29**(1), 25-40. https://doi.org/10.12989/gae.2022.29.1.025.

Wu, S.Y., Yang, X.P. and Liu, T.J. (2012), "Analysis of influence on deformation of adjacent subway tunnel due to bilateral deep excavations", *Chinese J. Rock Mech. Eng.*, **31**, 3452-3458.

Zhang, Q.B., He, L. and Zhu, W.S. (2016), "Displacement measurement techniques and numerical verification in 3D geomechanical model tests of an underground cavern group", *Tunn. Undergr. Sp. Tech.*, **56**, 54-64. https://doi.org/10.1016/j.tust.2016.01.029.

GC